Study on the expression level of folate receptor γ in thyroid cancer and its association with clinicopathological characteristics

JINYING CAO[1*], YANXU LI[2*], XIN DENG[1*], BO LV[1], LING HAN[1] and LING TONG[1,3]

[1]Chifeng Clinical Medical College of Inner Mongolia Medical University, Chifeng, Inner Mongolia Autonomous Region 024000, P.R. China; [2]Department of General Surgery, Chifeng Municipal Hospital, Chifeng, Inner Mongolia Autonomous Region 024000, P.R. China; [3]Department of Pathology, Chifeng Municipal Hospital, Chifeng, Inner Mongolia Autonomous Region 024000, P.R. China

Received May 30, 2025; Accepted December 8, 2025

DOI: 10.3892/ol.2026.15459

Abstract. Despite generally favorable outcomes, identifying reliable biomarkers remains crucial for managing aggressive subtypes of thyroid cancer. The present study aimed to investigate the association between folate receptor γ (FOLR3) expression and the clinicopathological features of thyroid cancer, and to explore its clinical relevance using bioinformatics and experimental approaches, ultimately assessing its potential value as a diagnostic and therapeutic biomarker. Differential expression analysis of RNA-sequencing data from The Cancer Genome Atlas database was performed to identify the differentially expressed gene FOLR3, followed by standard single-cell analysis. Clinicopathological data from 293 patients with thyroid cancer were collected to investigate pathological characteristics and FOLR3 expression, which was further validated using immunohistochemistry. The functional effects of FOLR3 on the malignant behavior of thyroid cancer cells were assessed using colony formation, Cell Counting Kit-8, scratch wound healing and Transwell invasion assays. FOLR3 expression was significantly higher in normal thyroid tissue compared with cancer tissues (P<0.001). FOLR3 expression level was associated with capsular invasion, perineural invasion, striated muscle invasion and pT stage (all P<0.05). Functional experiments demonstrated that FOLR3 suppressed the proliferation, migration and invasion of TPC-1 cells (all P<0.05). In conclusion, FOLR3 expression is generally low or absent in thyroid cancer, particularly in cases demonstrating pronounced local infiltration, indicating its potential as a diagnostic biomarker for the evaluation of tumor invasiveness. Patients with high FOLR3 expression exhibit a higher survival rate, suggesting its potential prognostic value. FOLR3 inhibits the progression of thyroid cancer by inhibiting the STAT3/MAPK signaling pathways and reprogramming folate metabolism, highlighting its potential as a therapeutic target for thyroid cancer in the future.

Correspondence to: Ms. Ling Tong, Department of Pathology, Chifeng Municipal Hospital, 11 Zhaowuda Road, Hongshan, Chifeng, Inner Mongolia Autonomous Region 024000, P.R. China
E-mail: tongling007@163.com

*Contributed equally

Key words: thyroid cancer, folate receptor γ, proliferation, migration

Introduction

Thyroid cancer ranks among the malignancies with the most rapidly increasing incidence. In the United States, its age-standardized incidence rate nearly tripled from 1975-1979 to 2015-2019. This trend has been particularly prominent among female patients in large urban areas, with the incidence among female patients rising from 7.8 to 29.5/100,000 during the same period, making it one of the most common cancer types in female patients (1,2). Although early-stage thyroid cancer is generally associated with favorable outcomes following timely diagnosis and treatment, the 5-year relative survival rate is ~98.5%, advanced disease accompanied by local invasion and distant metastasis remains a key challenge, often leading to poor prognosis (3). Thus, elucidating the molecular mechanisms underlying thyroid cancer progression and identifying relevant biomarkers are key for the enhancement of diagnostic accuracy and therapeutic strategies.

Folate receptor γ (FOLR3) is a key member of the folate receptor family. FOLR3 belongs to a soluble receptor subtype that serves a key role in the uptake and utilization of extracellular folic acid (4). Folate serves a dual role in cancer. On the one hand, folate may help prevent the development of certain cancer types. Previous studies have suggested that high folate intake is associated with a reduced risk of breast, colorectal and ovarian cancer types, making it a candidate for targeted cancer therapy (5-8). By contrast, folate may also promote cancer progression, for example, certain studies indicate that it might accelerate the development of prostate cancer (9,10). Dietary folate promotes hepatocellular carcinoma progression by hijacking methionine metabolism through VCIP135-mediated stabilization of methionine adenosyltransferase IIα, thereby coupling one-carbon and methionine metabolic flux to fuel tumor growth (11). The abnormal expression of FOLR3 may contribute to tumorigenesis and progression by interfering with folate metabolism, affecting DNA synthesis, methylation and cell proliferation. Furthermore, FOLR3 can exert antimicrobial and antitumor effects by sequestering natural

folate, thereby depriving bacteria and tumor cells of this vital nutrient (12,13). Although evidence suggests that FOLR3 is involved in cancer pathogenesis, its specific function in thyroid cancer remains poorly understood (14-17). Therefore, investigating the expression level of FOLR3 in thyroid cancer and its association with clinicopathological features may offer novel biomarkers for early diagnosis and prognosis evaluation of thyroid cancer.

Materials and methods

Bioinformatic analysis. Gene expression data for thyroid cancer were obtained from The Cancer Genome Atlas (TCGA; portal.gdc.cancer.gov/) database and the Gene Expression Omnibus (GEO; ncbi.nlm.nih.gov/geo/) dataset GSE250521 (18). From TCGA, the Thyroid Carcinoma project dataset was downloaded via the Genomic Data Commons Data Portal, which includes RNA-Seq data from tumor and adjacent normal tissue. The combined dataset included clinical information for 572 individuals, comprising of 513 thyroid cancer cases and 59 normal controls. Differential gene expression analysis was performed using the 'limma' package in the R software (version 3.64.1; R Development Core Team) (19), with a significance threshold set at adjusted $P<0.05$ and $|\log_2FC|>2.5$. Genes with $\log_2FC>2.5$ were considered upregulated, those with $\log_2FC<-2.5$ were classified as downregulated and genes with values between -2.5 and 2.5 were regarded as unchanged. Functional enrichment analyses, including Gene Ontology (GO) and Kyoto Encyclopedia of Genes and Genomes (KEGG) pathway analyses were performed using the 'clusterProfiler' package (version 4.16.0) in R (20). Univariate Cox regression analysis and multivariate Cox regression analysis were performed using the 'survival' (version 3.8-3) and 'survminer' packages (version 0.4.9) in R (21). Furthermore, FOLR3 expression in thyroid cancer was evaluated using the GEPIA2.0 (gepia.cancer-pku.cn) and University of Alabama at Birmingham Cancer data analysis Portal (ualcan.path.uab.edu/index.html) databases. For immune/stromal infiltration analysis, Cell-type Identification by Estimating Relative Subsets of RNA Transcripts (CIBERSORT) estimated immune cell proportions via deconvolution, while ESTIMATE calculated immune and stromal scores from signature gene sets (22,23). Together, they provide a comprehensive tumor microenvironment (TME) composition profile.

The single-cell gene expression matrix was preprocessed using the 'Seurat' R package (version 4.4.0) to ensure data quality and prepare for downstream analyses (24). Cell filtering was performed by retaining cells that met the following criteria: Detection of ≥500 genes, presence in ≥3 cells with non-zero unique molecular identifier (UMI) counts and a mitochondrial UMI ratio <25%. Genes detected in <3 cells were excluded. Highly variable genes were selected for dimensionality reduction via principal component analysis and the top 30 principal components were used for Uniform Manifold Approximation and Projection to visualize high-dimensional gene expression patterns in two dimensions. The Harmony algorithm was applied to correct for batch effects and minimize technical variability (25). Cell clustering was performed using the 'FindClusters' function with a resolution parameter of 0.7 to identify distinct cell populations. Differential expression analysis across cell subpopulations was conducted with the 'FindAllMarkers' function using the Wilcoxon rank-sum test and P-values were adjusted for multiple analysis with the false discovery rate (FDR) correction. Cell-cell communication analysis was carried out with the 'CellChat' package (version 1.6.1) to predict ligand-receptor interactions (26). Folate metabolism-related gene sets were obtained from the Molecular Signatures database and pathway activity scores were calculated using the 'AddModuleScore' function (27). Cells were stratified into high- and low-score groups based on the median pathway score, with a cutoff of 0.108. Myeloid cell subpopulations were annotated using the same workflow and analytical methods.

Clinical data. The present study included a total of 293 patients with thyroid cancer who were treated at Chifeng Hospital of Inner Mongolia (Chifeng, China) between January 2021 and June 2024. The cohort comprised 51 male and 242 women, with ages ranging from 19 to 78 years. According to the histopathological diagnosis, there were 287 cases of papillary thyroid carcinoma (PTC), 3 cases of follicular thyroid carcinoma and 3 cases of anaplastic thyroid carcinoma. The collected clinical and pathological parameters included sex, age, capsule invasion, perineural invasion, striated muscle cell infiltration, pathological tumor (pT) stage, tumor location, tumor focality, histological type, vascular infiltration and pathological lymph node (pN) stage, assessed according to the American Joint Committee on Cancer TNM staging system (8th edition) (28).

Construction of high-throughput thyroid tumor tissue microarray. Tissue samples were sourced from the surgical resection specimens of the 293 thyroid cancer patients. A manual tissue microarrayer was used to mark the tumor regions on large tissue sections. A 1 mm diameter core was extracted from each donor block and transferred into a recipient paraffin block to construct a high-throughput thyroid tumor tissue microarray. For each case, one core was taken from the tumor invasion front and one from adjacent normal thyroid tissue.

Immunohistochemical staining (IHC). Formalin-fixed, paraffin-embedded tissue sections (thickness, 4 μm) were used. Tissue samples were fixed in 10% neutral-buffered formalin at room temperature for 24-48 h. Antigen retrieval was performed using EnVision two-step method (95-100˚C, 15-20 min). Sections were dewaxed, rehydrated through a descending alcohol series (100, 95, 70% ethanol) to distilled water, and endogenous peroxidase activity was blocked with 3% hydrogen peroxide for 10 min at room temperature. Non-specific binding was blocked with 5% normal goat serum for 1 h at room temperature. Normal serum was incubated with rabbit anti-human FOLR3 antibody (1:100; cat. no. DF9519; Affinity Biosciences) overnight at 4˚C. After washing, EnVision HRP-conjugated goat anti-rabbit secondary antibody (1:100; Wuhan Proteintech, SA00001-2) was added for 30 min at room temperature, and DAB staining was used for color development. Hematoxylin re-dyeing for 2 min at room temperature. Phosphate buffer, isotype rabbit IgG (1:100, Wuhan Boster Biological Technology, Ltd.) instead of primary antibody were used as a negative control. Images were acquired using a light

microscope (Olympus Corporation) at x200 magnification. The percentage of cells positive for FOLR3 in thyroid cancer tissue vs. paired normal tissue was identified by QuPath software (version 0.4.4, QuPath) (29). The criteria for cytosol staining intensity was as follows: Negative, <0.20; 1, 0.2-0.39; 2, 0.40-0.6 and 3+, >0.6 (30). IHC results were evaluated using H-score method (31).

Cell culture. Human thyroid carcinoma TPC-1 cells (Abcells; cat. no. AC153) were cultured in complete medium (Seven Biotech) at 37˚C in a 5% CO_2 incubator (Thermo Fisher Scientific, Inc.). Cells were passaged every 2-3 days to maintain exponential growth.

Transfection. TPC-1 cells were seeded in 6-well plates and grown to ~70% confluence. The human FOLR3 overexpression plasmid (pcDNA3.1-hFOLR3-3XFLAG) and corresponding empty vector control (pcDNA3.1) were synthesized by Beijing Likeli Biotechnology Co., Ltd.). Cells were transfected with 2.5 μg FOLR3 overexpression or the empty control plasmid using 4 μl Lipo8000™ transfection reagent (Beyotime Biotechnology, C0533), according to the manufacturer's instructions. The transfection complexes were added at 37˚C. The culture medium was not replaced post-transfection. Transfected cells were harvested for subsequent experimentation 48 h post-transfection. Transfected cells were divided into two groups: Flag-FOLR3 group (FOLR3 overexpression) and the Flag-negative control (NC) group.

Reverse transcription-quantitative PCR (RT-qPCR). Total RNA was extracted from Flag-FOLR3 and NC groups using the RNAprep pure cell kit (Tiangen Biotech Co., Ltd.) and reverse transcribed into cDNA with the PrimeScript™ RT reagent kit (Takara Bio, Inc.). RT was performed at 37˚C for 15 min, followed by enzyme inactivation at 85˚C for 5 sec. RT-qPCR was using the Beyofast SYBR™ Green qPCR mix (Beyotime Biotechnology) on a Fluorescent Quantitative PCR Instrument (Bio-Rad). Thermocycling conditions were as follows: initial denaturation at 95˚C for 2 min, followed by 40 cycles of denaturation at 95˚C for 15 s and annealing/extension at 60˚C for 30 sec. The relative expression level of FOLR3 and folate metabolism-related genes was normalized to that of GAPDH, which served as the reference gene. All primers were designed and synthesized by Beyotime Biotechnology and quantification was performed using the $2^{-\Delta\Delta Cq}$ method (data not shown; Table I) (32). Each experiment was performed three times in duplicate.

Table I. Primer sequences.

Gene	Primer sequences (5'-3'
FOLR3	F: CGCAAAGAGCGCATTCTGAAC
	R: CTGGGCTGAGTCAAACCACA
GAPDH	F: ACGGATTTGGTCGTATGGG
	R: CGCTCCTGGAAGATGGTGAT
TYMS	F: TGATGGTGTCAATCACTCTTTGC
	R: TGGGGCAGAATACAGAGATATGG
MTHFR	F: GAGCGGCATGAGAGACTCC
	R: CCGGTCAAACCTTGAGATGAG
SLC19A1	F: CTCAGCTTCGTGTCGGTGT
	R: AGCGAGATGTAGTTGAGCGTG
PCFT	F: GGCCCAGGGTTATGCCAAC
	R: GGACAATGGATCGGTGGTGAC
Cyclin D1	F: CAATGACCCCGCACGATTTC
	R: CATGGAGGGCGGATTGGAA
Bcl-2	F: GGTGGGGTCATGTGTGTGG
	R: CGGTTCAGGTACTCAGTCATCC
c-FOS	F: GGGGCAAGGTGGAACAGTTAT
	R: CCGCTTGGAGTGTATCAGTCA
c-Jun	F: TCCAAGTGCCGAAAAAGGAAG
	R: CGAGTTCTGAGCTTTCAAGGT
VEGF	F: AGGGCAGAATCATCACGAAGT
	R: AGGGTCTCGATTGGATGGCA
MCL1	F: GTGCCTTTGTGGCTAAACACT
	R: AGTCCCGTTTTGTCCTTACGA

FOLR3, folate receptor γ; TYMS, thymidylate synthase; MTHFR, methylenetetrahydrofolate reductase; SLC19A1, solute carrier family 19 member 1; PCFT, proton-coupled folate transporter; c-FOS, Fos proto-oncogenes, AP-1 transcription factor subunit; MCL1, myeloid cell leukemia-1; F, forward; R, reverse.

Protein isolation and western blotting. TPC-1 cells were lysed using RIPA buffer (Beyotime Biotechnology) supplemented with PMSF (Beyotime Biotechnology) and homogenized mechanically until complete lysis was achieved. The lysate was centrifuged at 12,000 x g for 5 min at 4˚C to collect the supernatant. Protein concentration was determined using the Enhanced BCA Protein Assay Kit. Proteins (10 μg per lane) were separated by 10% SDS-PAGE and transferred to PVDF membrane. The membrane was blocked with 5% non-fat milk in TBST at room temperature for 1 h, the corresponding FOLR3 (1:2,000; Affinity Biosciences; cat. no. DF9519) and GAPDH antibody (1:2,000; Wuhan Boster Biological Technology, Ltd, BA1050) was added overnight at 4˚C. The membrane was washed and then the HRP-conjugated goat anti-rabbit secondary antibody (1:5,000; Wuhan Boster Biological Technology, Ltd, BM3874) was added for 1 h at room temperature. The indicator proteins were assessed using a hypersensitive ECL chemiluminescence kit (Seven Biotech) and the relative expression level of FOLR3 was normalized to GAPDH. Each experiment was performed three times in duplicate.

Scratch assay. After transfection, cells from the Flag-FOLR3 and NC groups were seeded at $1x10^6$ cells per well into 6-well plate until they reached 100% confluence. A scratch was made in each well using a sterile 200 μl pipette tip. Cells were washed and cultured in RPMI-1640 (Beijing Solarbio Science & Technology Co., Ltd.). Wound healing was observed and captured at 0, 24 and 48 h using an inverted microscope (Olympus Corporation). The migration distance was quantified using ImageJ software (version 1.53f; National Institutes of Health). Each experiment was performed three times in duplicate.

Cell Counting Kit-8 (CCK-8) assay. Transfected cells were seeded into 96-well plates. After culturing for 0, 24, 48, 72 and 96 h, enhanced CCK-8 (Beyotime Biotechnology) was added to each well. Following incubation for 1.5 h, the optical density value at 450 nm was measured using a microplate reader (Thermo Fisher Scientific, Inc.), Each experiment was performed three times in duplicate.

Clone formation assay. Transfected cells were seeded at 1,000 cells/well into 6-well plates and cultured for 14 days in a CO_2 incubator at 37˚C. Cells were fixed at room temperature with 4% paraformaldehyde (Beyotime Biotechnology) for 20 min and stained with 0.1% crystal violet solution (Beyotime Biotechnology) at room temperature for another 20 min. Each experiment was performed three times in duplicate.

Transwell invasion assay. The upper chamber of Transwell plates were pre-coated with Matrigel™ Basement Membrane Matrix (Beyotime Biotechnology) and incubated for 2 h at 37˚C. A cell suspension containing $5x10^4$ cells in 200 μl serum-free RPMI-1640 medium (Beijing Solarbio Science & Technology Co., Ltd.). was added to the upper chamber and 600 μl TPC-1 complete medium (Abcells) containing 10% FBS was placed in the lower chamber. Following incubation for 24 h at 37˚C in a 5% CO_2 incubator, cells that had invaded through the membrane were fixed with 4% paraformaldehyde at room temperature for 20 min, stained with 0.1% crystal violet at room temperature for 20 min and counted under a microscope. Each experiment was performed three times in duplicate.

Statistical analysis. Statistical analyses were performed using GraphPad Prism (version 8.0.2; Dotmatics), ImageJ (version 1.53f; National Institutes of Health) and SPSS software (version 23.0; IBM Corp.), and R software (version 4.2.3). Data from the IHC analysis are presented as mean ± SD. $P<0.05$ was considered statistically significant. In bioinformatic analyses, significance thresholds were set at $P<0.05$ and a false discovery rate (FDR) <0.05. For functional experiments, group comparisons were conducted as follows: the CCK-8 cell proliferation, scratch wound healing, colony formation and Transwell invasion assays were analyzed using unpaired Student's t-tests. Comparisons of FOLR3 expression between paired tumor and adjacent normal tissue in IHC were analyzed using paired Student's t-test. The associations between FOLR3 expression and clinicopathological features (including age, sex, tumor location, pT and pN stage, perineural and vascular invasion) were evaluated using the χ^2 or Fisher's exact test, as appropriate. Independent prognostic factors were identified using multivariate Cox regression analysis. All bioinformatic statistical computations, data processing and visualizations were performed using R software.

Results

Bioinformatics analysis of FOLR3 expression in thyroid cancer and normal adjacent tissue. Expression profiling analysis of thyroid cancer data from TCGA identified 520 differentially expressed genes (DEGs), including 235 up- and 285 downregulated genes. The distribution of these DEGs is visually represented in the volcano plot (Fig. 1A). GO enrichment analysis identified 24 enriched terms in the three major categories: Biological process, cellular component and molecular function, while KEGG pathway analysis revealed 10 significantly enriched pathways ($P<0.01$; Fig. 1B and C). GO enrichment analysis was primarily associated with 'neural synapse-related functions', 'extracellular matrix remodeling' and 'ion channel activity'. KEGG pathway analysis highlighted processes such as 'cell adhesion molecules', 'tyrosine metabolism', 'protein digestion and absorption' and 'complement and coagulation cascades'.

Furthermore, a least absolute shrinkage and selection operator (LASSO) regression model, developed using machine learning techniques was employed to identify genes associated with the progression and prognosis of thyroid cancer (Fig. 1D). The resulting LASSO regression model and the results of cross-validation results selected 10 relevant genes (integrin-binding sialoprotein, ATPase secretory pathway Ca^{2+} transporting 2, synapse differentiation induced gene 1, stathmin-2, FOLR3, LIM homeobox transcription factor 1-β, C-X-C motif chemokine ligand 5, neuroligin-1, family with sequence similarity 111, member B and zinc finger protein 560; Fig. 1E). FOLR3 was selected as a research focus as it is one of the significantly downregulated genes in thyroid cancer, and the LASSO regression model identified it as one of the ten key genes associated with disease progression and prognosis.

The present study results demonstrated that FOLR3 expression was significantly downregulated in thyroid cancer tissues compared with normal tissues ($P<0.001$; Fig. 1F). Survival analysis indicated that high expression level of FOLR3 was associated with significantly worse overall survival in patients with thyroid cancer ($P=0.0074$; Fig. 1G). Multivariate Cox regression analysis identified CXCL5 as a significant independent prognostic biomarker for thyroid cancer ($P=0.0047$; Fig. 1J). Comparative assessment of TME profiles revealed distinct immune and stromal features associated with FOLR3 expression levels and tissue status in thyroid cancer. ESTIMATE algorithm revealed low FOLR3 expression was associated with lower tumor purity ($P<0.001$) and higher immune scores (both $P<0.001$) and ESTIMATE scores ($P=0.0011$; Fig. 1H). Similarly, thyroid cancer tissues exhibited markedly lower immune and stromal infiltration overall compared with normal tissues (Fig. 1I). CIBERSORT-based immune deconvolution further illustrated divergent microenvironmental landscapes. High FOLR3 expression was associated with increased infiltration of antitumor immune subsets, including plasma cells ($P=0.0415$), $CD8^+$ T cells ($P=0.0027$). By contrast, low FOLR3 expression favored an immunosuppressive milieu, characterized by elevated naïve $CD4^+$ memory T cells ($P=0.043$), M0 macrophages ($P=0.0005$) and activated mast cells ($P=0.0078$) (Fig. 1K). Thyroid cancer tissues displayed enriched infiltration of immunosuppressive cells, such as resting Tregs ($P=0.023$), M2 macrophages ($P=0.431$), resting dendritic cells ($P=0.0042$) and resting mast cells ($P=0.0011$), compared with normal tissues, indicating an overall immunosuppressive TME ($P<0.001$) (Fig. 1L). These results collectively indicate that FOLR3 expression is closely associated with immune-active microenvironment phenotypes, while its downregulation may contribute to an immunosuppressive TME in thyroid cancer.

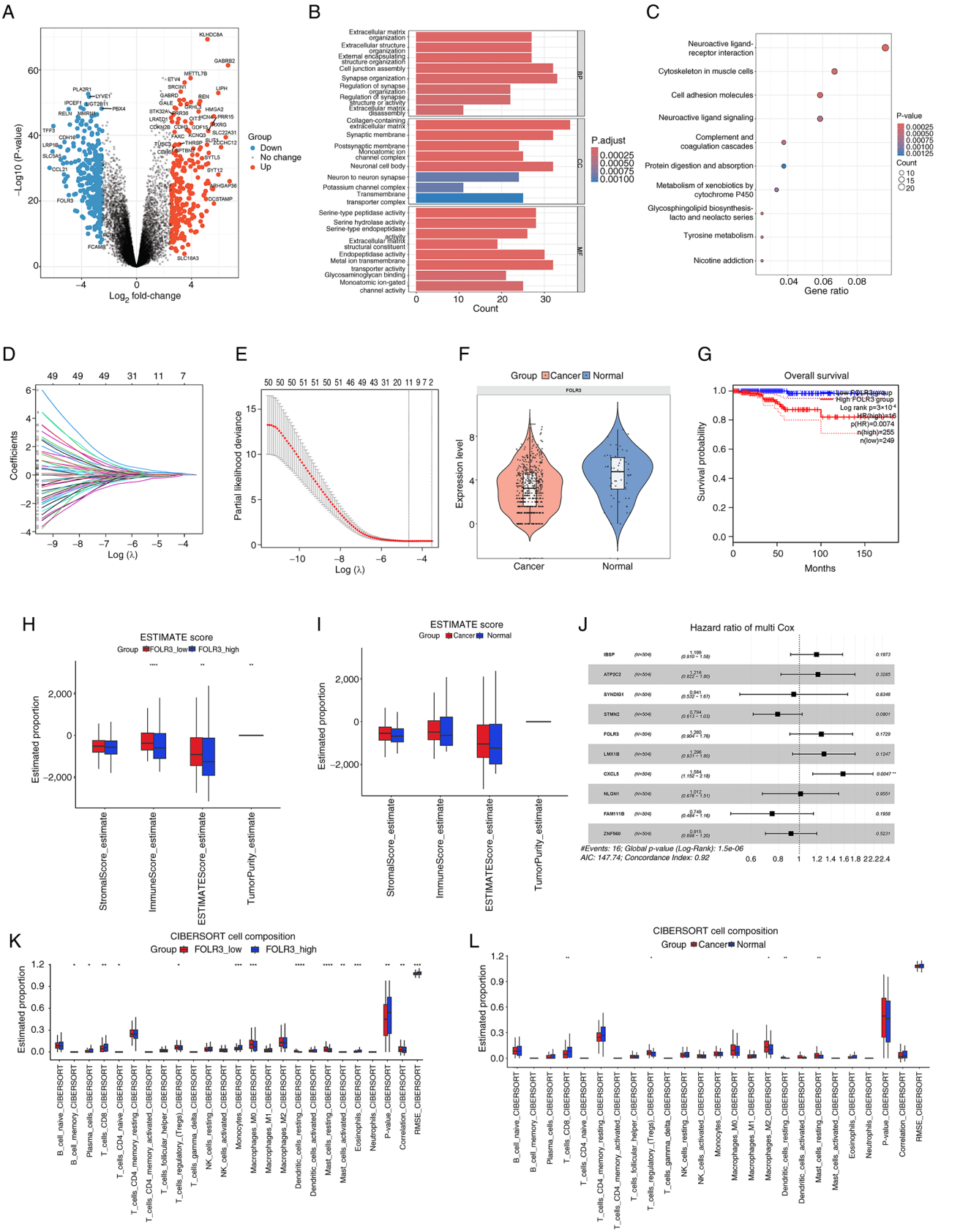

Figure 1. Analysis of FOLR3 expression and its impact in thyroid cancer. (A) Volcano plot of DEGs (red, upregulated; blue, downregulated). (B) GO enrichment analysis demonstrating three major functional categories. (C) KEGG pathway enrichment of DEGs. (D) LASSO regression model for feature selection. (E) A 10-fold cross-validation curve for the LASSO model. (F) FOLR3 expression levels in thyroid cancer vs. normal tissue. (G) Survival analysis based on FOLR3 expression. (H) ESTIMATE scores comparing high vs. low FOLR3 expression groups. (I) ESTIMATE scores in thyroid cancer vs. normal tissues. (J) Univariate Cox regression analysis of prognostic factors. (K) CIBERSORT analysis of immune infiltration in high vs. low FOLR3 expression groups. (L) CIBERSORT analysis of immune infiltration in thyroid cancer vs. normal tissues. *P<0.05, **P<0.01, ***P<0.001 and ****P<0.0001. FOLR3, folate receptor γ; GO, Gene Ontology; KEGG, Kyoto Encyclopedia of Genes and Genomes; LASSO, least absolute shrinkage and selection operator; CIBERSORT, Cell-type Identification by Estimating Relative Subsets of RNA Transcripts; DEGs, differentially expressed genes.

Remodeling of the TME in PTC: Metabolic reprogramming, immune activation and altered cellular communication driven by folate-high M1 macrophages. The present study comprehensively characterized the TME of PTC through integrated analysis of single-cell transcriptomic data and functional enrichment. The PTC dataset GSE250521 was downloaded from the GEO database. After quality control and normalization, the dataset contained 33,505 cells and 31,454 genes. Manual annotation of the main cell subsets revealed six distinct populations: Thyrocytes [thyroglobulin (TG), epithelial cell adhesion molecule, keratin (KRT) 18 and KRT19], fibroblasts (collagen type I α 1 chain, collagen type I α 2 chain, collagen type III α 1 chain and actin, α 2, smooth muscle), endothelial cells (platelet-endothelial cell adhesion molecule 1, CD34, cadherin 5 and von Willebrand factor), T/natural killer (NK) cells (CD3D, CD3E, CD3G and CD247), B cells (CD79A, CD79B, immunoglobulin heavy constant μ and immunoglobulin heavy constant Δ) and myeloid cells (lysozyme, S100 calcium binding protein A8, S100 calcium binding protein A9 and CD14) (Fig. 2A and B).

Key findings revealed extensive remodeling of the TME in PTC, beginning with a marked shift in cellular composition: The present study observed a marked decrease in thyrocytes and a concurrent increase in myeloid cells, indicative of enhanced stromal and immune infiltration accompanied by loss of functional thyroid epithelium (Fig. 2C). Further analysis identified elevated folate metabolism activity as a hallmark of PTC, particularly within myeloid cells. Notably, M1 macrophages not only demonstrated the highest folate metabolic score among all subsets but also constituted the majority of cells within the high folate metabolism group (Fig. 2D, H and I). Sub-clustering of myeloid cells confirmed the expansion of M1 macrophages in PTC (Fig. 2F and G) and these cells exhibited pronounced enrichment of immune-inflammatory pathways, including TNF-α, IFN-γ, KRAS and NF-κB signaling, allograft rejection, epithelial-mesenchymal transition and complement activation (Fig. 2J, N and O). Cell communication analysis revealed that M1 macrophages undergo the most notable alterations in both the number and strength of interactions, notably with T/NK cells and engage key ligand-receptor axes such as secreted phosphoprotein 1-CD44, TNF-TNF receptor superfamily, macrophage migration inhibitory factor-(CD74$^+$/CD44/C-X-C motif chemokine receptor 4) and IL6-IL6 receptor, which are key in inflammation, adhesion and immune regulation (Fig. 2E, K and M). In addition, signaling network inference highlighted 'RESISTIN', 'MK' and 'GDF' pathways as key mediators of intercellular crosstalk within the TME (Fig. 2L). Collectively, these results underscore the dual role of M1 macrophages in PTC, mechanistically associating folate metabolism with pro-tumorigenic inflammation and immune modulation and identifying them as pivotal regulators of TME remodeling.

Expression of FOLR3 protein in thyroid cancer and adjacent normal tissue. IHC revealed that FOLR3 expression was significantly higher in normal thyroid tissues (H-score, 129.93±50.18) compared with thyroid cancer tissues (H-score, 99.68±47.67) (Table II; Fig. 3). A paired t-test confirmed that this difference was statistically significant (P<0.0001; Table II).

Association analysis of FOLR3 and clinicopathological factors in thyroid cancer. The expression levels of FOLR3 were significantly associated with capsule invasion, neurofibrillary invasion, striated muscle cell invasion and pT stage (P<0.05) and there was no significant association with sex, age, tumor location, tumor focality, histological type, vascular invasion or pN stage (P<0.05) (Table III). FOLR3 was commonly downregulated or absent in cases with capsule, rhabdomyocyte invasion or larger tumor burden, suggesting that FOLR3 could serve as an indicator of focal invasion in thyroid cancer.

FOLR3 inhibits proliferation, invasion and migration of thyroid cancer TPC-1 cells. The western blotting analysis (Fig. 4A and B) confirmed successful overexpression of FOLR3 protein in TPC-1 cells of the Flag-FOLR3 group compared with the NC (P<0.01). RT-qPCR results demonstrated a significant upregulation of FOLR3 mRNA expression in the Flag-FOLR3 group (P<0.0001; Fig. 4C). Colony formation assays demonstrated the clonogenic ability of Flag-FOLR3 group was significantly lower compared with that of NC group (P<0.05), indicating that FOLR3 overexpression impaired the proliferative capacity of TPC-1 cells (Fig. 4E and F). The results of the scratch assay demonstrated cell migration was significantly attenuated in the Flag-FOLR3 group compared with the NC group at both 24 (P<0.05) and 48 h (P<0.001), confirming that FOLR3 overexpression suppresses the migratory ability of TPC-1 cells (Fig. 4G and H). Similarly, Transwell invasion assays indicated that the invasive capacity of TPC-1 cells was significantly reduced in the Flag-FOLR3 group after 24 h (P<0.01), indicating that FOLR3 overexpression significantly inhibits cell invasion (Fig. 4I and J). CCK-8 assays indicated that TPC-1 cell proliferation was significantly inhibited at 48, 72 and 96 h after FOLR3 overexpression (P<0.05; Fig. 4D).

FOLR3 overexpression suppresses the progression of thyroid cancer by inactivating the STAT3/MAPK signaling pathways and subsequently reprogramming folate metabolism. To elucidate the molecular mechanism underlying the tumor-suppressive role of FOLR3, the present study first investigated its impact on folate metabolism using qPCR analysis. Notably, FOLR3 overexpression significantly downregulated the mRNA level of the folate transporter gene solute carrier family 19 member 1 and upregulated that of solute carrier family 46 member 1 (P<0.05). Concurrently, expression levels of key folate metabolic enzyme genes, methylenetetrahydrofolate reductase and thymidylate synthase, were significantly downregulated (P<0.05). These results indicate that FOLR3 overexpression induces notable reprogramming of folate metabolism in thyroid cancer cells (Fig. 5A), which may contribute to the inhibition of tumor progression.

The present study further examined whether FOLR3 modulates oncogenic signaling pathways by assessing the expression levels of downstream effectors of STAT3 and MAPK signaling. RT-qPCR revealed that overexpression of FOLR3 significantly downregulated both mRNA and protein levels of myeloid cell leukemia-1 (MCL1), an anti-apoptotic gene downstream of STAT3 (P<0.05). Similarly, expression levels of cyclin D1, a key cell cycle regulator mediated by the

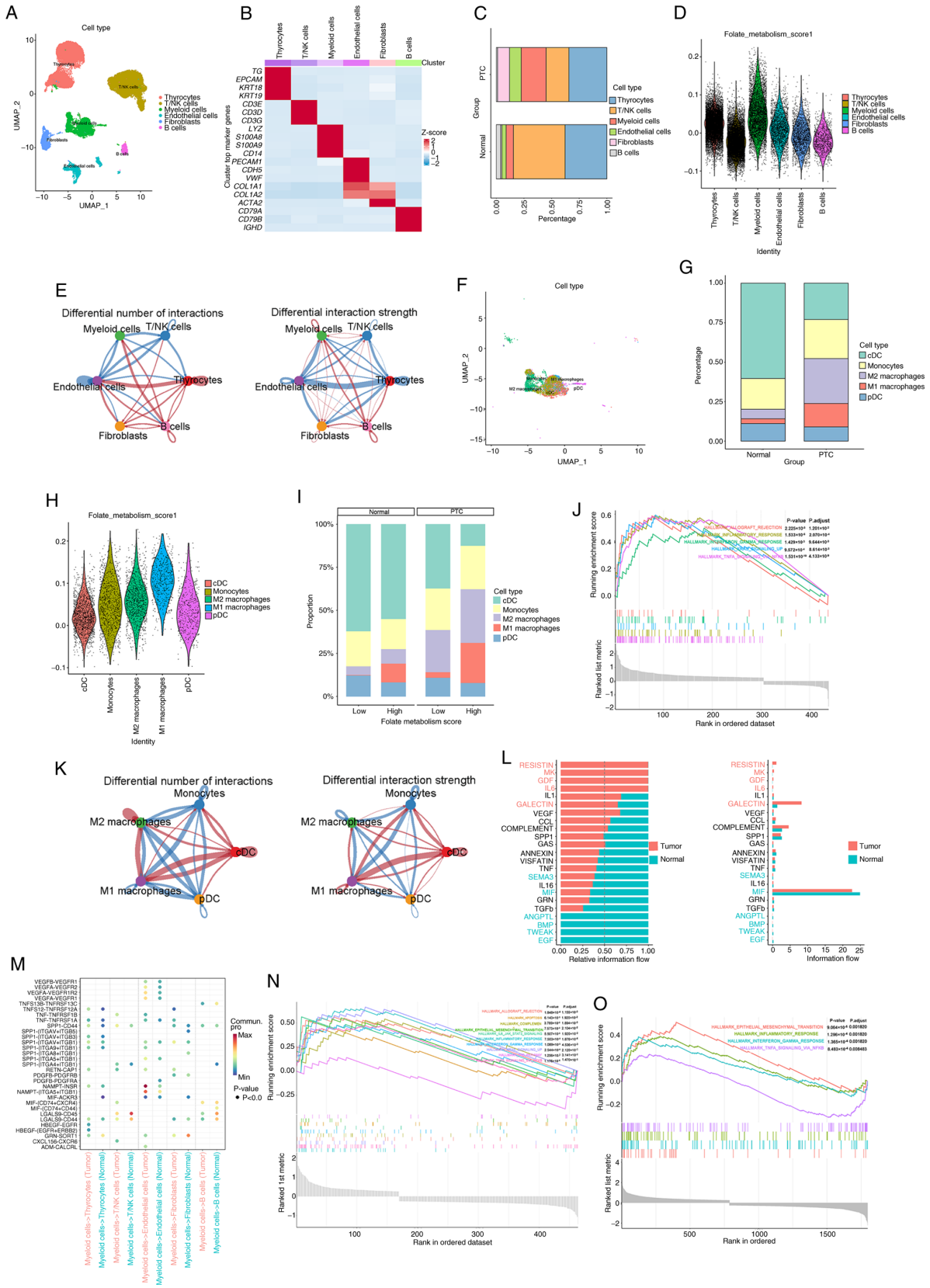

Figure 2. Single-cell transcriptomic profiling reveals metabolic-immune remodeling in the tumor microenvironment of papillary thyroid carcinoma. (A) UMAP visualization of single-cell RNA sequencing data from PTC and normal thyroid tissues. (B) Expression levels of canonical marker genes across major cell types. (C) Altered cellular composition in PTC vs. normal tissues. (D) Folate metabolism scores of major cell types. (E) Differential cell-cell interactions within the TME. (F) Re-annotation of myeloid cell subpopulations. (G) Altered proportions of myeloid subsets in PTC. (H) Heterogeneity in folate metabolism scores among myeloid subpopulations. (I) Distribution of myeloid subsets stratified by folate metabolism score and tissue type. (J) Top five enriched Hallmark pathways in myeloid cells. (K) Altered intercellular communication among myeloid subpopulations. (L) Signaling pathways ranked by intercellular communication activity. (M) Key ligand-receptor interactions involving M1 macrophages. (N) Comparison of Hallmark pathways significantly enriched in macrophages with high vs. low folate metabolic status. (O) Significantly enriched Hallmark pathways in high folate metabolism myeloid cells and M1 macrophages. FOLR3, folate receptor γ; UMAP, Uniform Manifold Approximation and Projection; PTC, papillary thyroid carcinoma; TME, tumor microenvironment.

Table II. H-scores of the patients (n=293).

Patient no.	Normal thyroid tissues	Thyroid cancer tissues
1	164.55	146.37
2	146.00	136.58
3	133.02	129.21
4	247.31	195.57
5	148.17	87.76
6	160.78	138.36
7	114.05	53.49
8	211.47	154.97
9	193.39	153.36
10	154.94	145.04
11	150.71	143.13
12	183.65	98.63
13	171.79	153.39
14	151.49	146.88
15	201.25	154.38
16	186.21	151.62
17	116.70	104.32
18	152.38	126.82
19	162.38	148.82
20	171.70	61.32
21	125.82	72.99
22	215.35	172.70
23	219.23	147.34
24	171.05	156.03
25	196.15	161.93
26	184.15	111.95
27	181.24	139.55
28	133.28	126.86
29	204.96	149.66
30	143.99	132.18
31	174.22	145.96
32	156.80	139.17
33	86.04	54.02
34	108.69	109.10
35	119.19	82.42
36	109.45	77.76
37	108.59	57.18
38	99.96	51.16
39	86.40	40.47
40	96.69	46.96
41	122.83	108.76
42	158.93	113.31
43	140.82	118.09
44	105.50	63.45
45	131.70	111.66
46	139.03	86.48
47	94.88	68.67
48	56.94	39.40
49	85.17	48.56
50	11.55	8.62
51	135.13	132.38

Table II. Continued.

Patient no.	Normal thyroid tissues	Thyroid cancer tissues
52	147.64	137.57
53	127.17	119.15
54	92.66	103.77
55	134.85	84.52
56	96.37	39.76
57	54.15	42.18
58	65.47	13.09
59	63.74	1.07
60	5.88	0.18
61	113.42	91.81
62	210.17	64.71
63	190.18	122.17
64	88.44	70.45
65	116.35	157.87
66	76.91	56.08
67	159.75	68.34
68	156.54	119.36
69	160.64	136.02
70	59.53	55.13
71	81.79	78.75
72	93.73	50.22
73	130.00	39.09
74	87.28	41.11
75	216.87	103.31
76	98.67	74.03
77	99.00	73.30
78	90.94	79.29
79	164.41	93.89
80	167.83	166.5
81	137.57	69.51
82	111.62	49.47
83	201.42	134.27
84	163.93	118.29
85	80.09	61.97
86	192.61	88.74
87	170.62	152.33
88	191.49	50.53
89	119.56	119.22
90	67.67	45.43
91	67.53	51.54
92	106.34	6.95
93	120.59	35.01
94	61.15	38.78
95	120.41	89.81
96	50.26	16.43
97	62.52	42.29
98	48.86	25.90
99	35.35	24.36
100	113.82	113.06
101	73.47	64.73
102	81.64	76.59

Table II. Continued.

Patient no.	Normal thyroid tissues	Thyroid cancer tissues
103	61.18	14.07
104	74.41	28.97
105	112.23	58.89
106	75.94	45.13
107	116.07	93.56
108	99.80	58.09
109	92.19	22.33
110	42.86	12.04
111	10.30	11.21
112	124.12	50.37
113	85.12	42.66
114	83.75	74.22
115	32.02	14.77
116	84.79	90.94
117	73.23	96.52
118	1.33	8.67
119	117.84	96.20
120	66.44	56.91
121	95.26	97.71
122	127.92	76.75
123	73.33	79.05
124	56.06	45.97
125	117.35	76.76
126	100.10	44.13
127	126.63	110.81
128	131.09	100.99
129	30.80	28.38
130	101.37	82.66
131	64.22	55.62
132	51.98	35.75
133	172.32	64.74
134	67.35	60.24
135	58.16	41.55
136	33.55	33.89
137	85.79	60.32
138	26.20	5.91
139	34.32	10.65
140	59.71	42.04
141	188.62	104.21
142	45.80	31.95
143	147.59	75.87
144	70.59	38.08
145	84.66	59.77
146	108.32	87.49
147	71.66	57.89
148	80.62	134.46
149	137.00	116.60
150	140.84	139.98
151	134.13	81.44
152	135.82	131.41
153	185.20	161.26

Table II. Continued.

Patient no.	Normal thyroid tissues	Thyroid cancer tissues
154	158.57	147.50
155	147.48	132.21
156	180.52	95.11
157	78.38	66.41
158	161.33	154.09
159	111.38	106.17
160	184.15	152.06
161	148.90	142.03
162	190.60	167.59
163	194.39	152.33
164	166.85	154.07
165	158.80	141.93
166	188.04	187.25
167	143.03	89.98
168	162.27	148.97
169	168.05	176.93
170	127.95	117.53
171	147.88	116.69
172	112.18	102.63
173	164.60	29.74
174	124.81	106.56
175	104.00	71.29
176	80.54	58.33
177	39.82	18.88
178	100.87	44.71
179	96.21	69.35
180	133.71	71.09
181	69.68	51.30
182	106.75	86.33
183	131.84	64.39
184	71.89	23.83
185	132.16	39.71
186	129.86	45.19
187	52.52	49.63
188	86.69	99.01
189	96.55	66.90
190	39.05	5.49
191	57.76	52.49
192	78.92	66.92
193	53.93	49.64
194	114.65	100.65
195	84.82	65.47
196	111.75	101.47
197	80.33	94.78
198	108.18	73.45
199	76.27	77.60
200	112.31	68.72
201	80.01	58.27
202	89.42	72.15
203	96.58	79.57
204	102.38	69.58

Table II. Continued.

Patient no.	Normal thyroid tissues	Thyroid cancer tissues
205	97.33	70.65
206	93.90	76.41
207	117.50	60.98
208	23.55	3.58
209	157.45	107.52
210	81.05	60.24
211	137.02	116.14
212	118.78	79.55
213	133.41	133.66
214	164.76	116.36
215	180.06	182.92
216	166.59	118.32
217	170.52	170.16
218	193.79	163.37
219	193.36	158.70
220	187.24	170.76
221	183.74	145.64
222	182.94	172.33
223	131.85	89.28
224	148.43	77.22
225	166.30	160.53
226	150.27	142.50
227	135.90	81.77
228	146.95	133.12
229	151.41	150.12
230	143.85	133.38
231	99.93	43.97
232	151.49	121.59
233	144.99	124.87
234	142.00	122.68
235	165.83	140.79
236	208.44	187.60
237	178.17	163.92
238	168.91	141.85
239	165.80	145.45
240	136.95	139.40
241	147.78	135.69
242	105.73	86.53
243	73.78	0.95
244	97.68	47.81
245	163.53	57.35
246	166.40	107.74
247	129.13	108.89
248	137.95	112.03
249	143.59	109.13
250	137.34	132.70
251	175.34	147.97
252	184.94	172.82
253	156.07	143.52
254	189.84	188.35
255	183.57	169.42

Table II. Continued.

Patient no.	Normal thyroid tissues	Thyroid cancer tissues
256	168.51	138.99
257	127.93	118.84
258	158.56	143.35
259	123.80	105.50
260	194.29	135.53
261	159.92	99.10
262	131.32	120.29
263	48.63	30.04
264	164.66	127.32
265	127.74	77.67
266	101.59	88.66
267	128.55	117.84
268	100.90	57.06
269	134.81	87.24
270	134.47	110.14
271	118.35	109.63
272	131.51	111.68
273	126.47	120.74
274	243.09	132.76
275	138.70	112.34
276	215.87	91.34
277	163.43	113.18
278	192.07	133.95
279	177.21	123.38
280	174.17	112.87
281	152.79	121.19
282	130.25	125.07
283	182.06	170.84
284	163.29	152.19
285	142.50	133.29
286	135.76	112.89
287	162.53	132.69
288	164.47	133.78
289	114.49	115.11
290	183.97	136.89
291	158.09	88.39
292	98.89	63.07
293	160.68	47.88

P<0.0001. The mean H-score was significantly higher in normal tissues (129.93±50.18) than in cancer tissues (99.68±47.67).

MAPK pathway, were also significantly suppressed (P<0.05; Fig. 5B and C). These findings demonstrated that FOLR3 overexpression effectively inhibits the activity of both STAT3 and MAPK signaling pathways. Collectively, the present study results suggest that FOLR3 constrains thyroid cancer development through dual mechanisms: Inactivation of STAT3 and MAPK signaling pathways and concomitant reprogramming of folate metabolism.

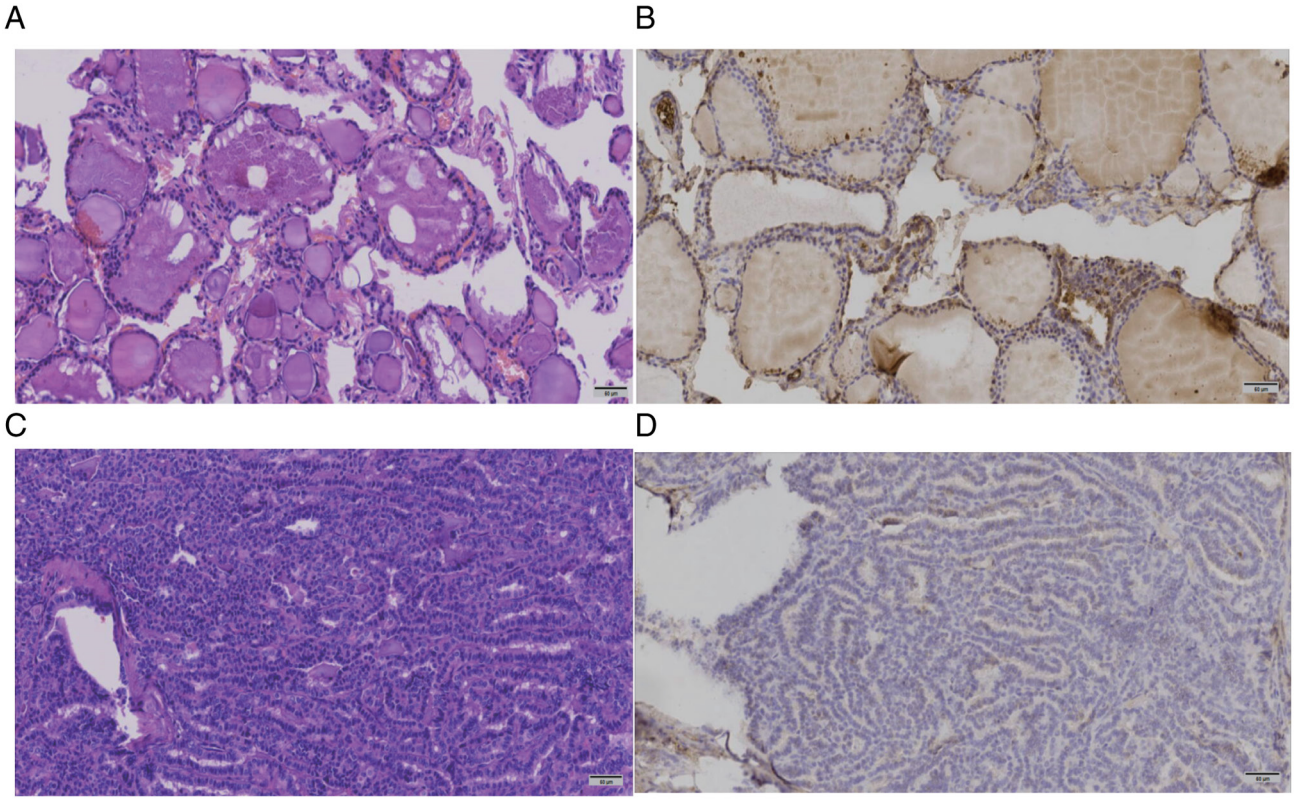

Figure 3. Immunohistochemical analysis of FOLR3 expression in thyroid tissues. (A) H&E staining of normal thyroid tissue. (B) IHC staining demonstrating high FOLR3 expression in normal thyroid tissue. (C) H&E staining of thyroid cancer tissue. (D) IHC staining demonstrating weak or absent FOLR3 expression in thyroid cancer tissue. Magnification, x200. FOLR3, folate receptor γ; IHC, immunohistochemistry.

Discussion

Thyroid cancer is one of the fastest-growing malignancies in recent years, with a notably higher incidence among women (33,34). Despite the notable improvements in early diagnosis and treatment, patients with advanced thyroid cancer still face poor prognosis due to tumor invasiveness and metastasis (35,36). Therefore, understanding the molecular mechanisms underlying thyroid cancer and identifying novel biomarkers are key to the improvement of diagnosis, treatment and prognosis. To the best of our knowledge, the present study investigated the expression level of FOLR3 in thyroid cancer and its association with clinicopathological features, for the first time. FOLR3, a member of the folate receptor family, has been implicated in various cancer types (37-39). In tongue cancer, FOLR3 is an upregulated immune-related target associated with patient prognosis (37). Similarly, its expression is upregulated in metastatic uterine leiomyosarcoma compared to primary tumors, suggesting a potential role in promoting metastatic disease (38). Furthermore, transcriptomic analysis of peripheral blood mononuclear cells from patients with head and neck squamous cell carcinoma revealed FOLR3 as one of the differentially expressed genes, indicating its systemic involvement in cancer-related immune responses (39). The present bioinformatics analysis and experimental data revealed that FOLR3 is significantly downregulated in thyroid cancer tissues compared with normal tissue and its high expression was associated with worse overall survival. The seemingly contradictory link between FOLR3 expression and clinical prognosis may be explained by its cell type-specific functions within the tumor microenvironment. While FOLR3 is typically downregulated in cancer cells (a tumor-suppressive effect), its high overall levels in tumors mainly comes from tumor-infiltrating immune cells such as macrophages. This immune-derived FOLR3 enrichment is indicative of an immunosuppressive tumor microenvironment that promotes disease progression and is associated with poorer patient survival. Therefore, FOLR3 exhibits a dual function, acting as a putative tumor suppressor within cancer cells while serving as a biomarker and functional driver of an immune-favorable, pro-tumorigenic niche (12,37-41). Therefore, FOLR3 has the potential for targeted therapy.

Single-cell transcriptomic analysis revealed a significant expansion of M1 macrophages with heightened folate metabolism in the TME of PTC. These folate-high M1 macrophages drive TME remodeling and promote pro-tumor inflammatory responses through activation of immune-inflammatory pathways and enhanced intercellular communication. Mechanistically, FOLR3 suppresses thyroid cancer growth by inactivating the STAT3 and MAPK signaling pathways through downregulation of their key downstream oncogenes, MCL1 and cyclin D1, ultimately leading to reprogramming of folate metabolism. Notably, FOLR3 has also been reported to influence other cancer types. Recent studies have reported that FOLR3 undergoes hypomethylation in the blood of patients with non-small cell lung cancer and lung adenocarcinoma, suggesting that FOLR3 hypomethylation could serve as an early diagnostic marker for these cancers (12,40). Furthermore, high expression of FOLR3 in patients with laryngeal squamous cell

Table III. Association between FOLR3 expression and clinicopathological parameters in patients with thyroid cancer (n=293).

		FOLR3 expression		
Clinicopathological feature	No. of cases	Low, n	High, n	P-value
Sex				0.465
Male	51	29	22	
Female	242	124	118	
Age, years				0.165
≤65	282	145	137	
>65	11	8	3	
Tumor location				0.473
Unilateral	255	129	126	
Bilateral	38	18	20	
Histological type				0.832
Papillary carcinoma	287	145	142	
Follicular carcinoma	3	1	2	
Anaplastic cancer	3	1	2	
Tumor focality				0.446
Single lesion	165	80	85	
Multiple lesions	128	67	61	
Capsule invasion				0.042[a]
No	102	45	57	
Yes	191	108	83	
Rhabdomyocyte invasion				0.006[a]
Yes	285	145	140	
No	8	8	0	
pT stage				0.047[a]
1	272	141	131	
2	14	5	9	
3	5	5	0	
4	2	2	0	
pN stage				0.864
0	168	87	81	
1	125	66	59	
Vascular invasion				0.123
No	287	148	139	
Yes	6	5	1	
Perineural invasion				0.025[a]
No	284	145	139	
Yes	9	8	1	

[a]P<0.05. pN, pathological lymph node stage; pT, pathological tumor stage. FOLR3, folate receptor γ.

carcinoma after chemotherapy has been reported to influence subsequent treatment strategies (41). These findings across cancer types reinforce the biological and clinical relevance of FOLR3 and support the present study results highlighting its importance in thyroid cancer.

The human body expresses three isoforms of folate receptors (FOLRs): FOLR1, FOLR2 and FOLR3, which have distinct distributions, structures and functions. Both FOLR1 and FOLR2 are glycosylphosphatidylinositol (GPI)-anchored membrane proteins that lack transmembrane domains, whereas FOLR3 is secreted into extracellular compartments, such as blood and breast milk, in a soluble form due to the absence of a GPI-anchoring signal (42,43). FOLR1 mainly facilitates folate endocytosis to support classical folate-dependent proliferative pathways. Although FOLR1 is upregulated in various types of cancers including ovarian cancer , Non-Small Cell Lung cancer and rectal cancer, and is generally associates with accelerated tumor progression and poor prognosis, its specific role

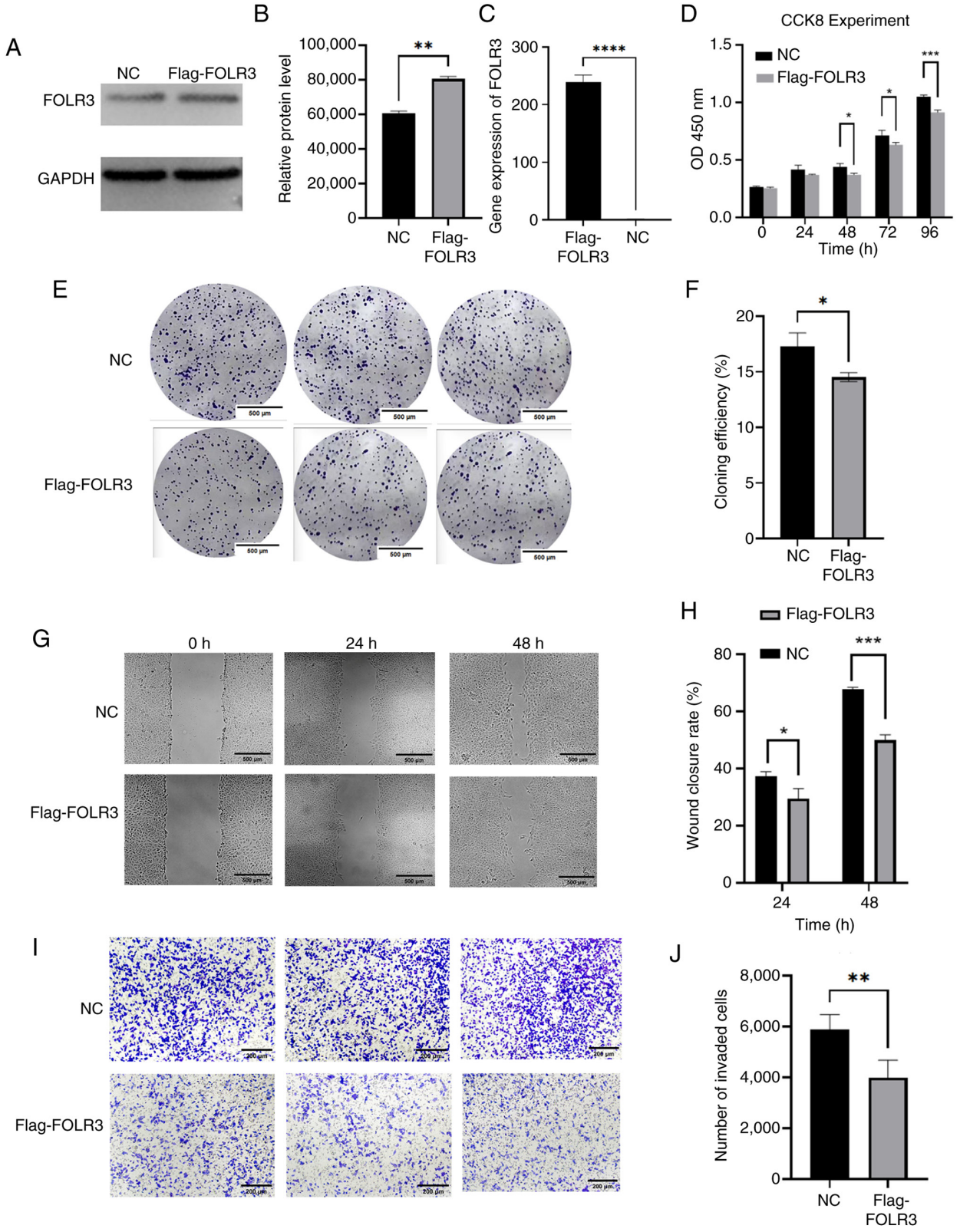

Figure 4. Functional characterization of FOLR3 in thyroid cancer cells *in vitro*. (A) Protein expression levels of FOLR3 assessed using western blotting and (B) semi-quantification. (C) Relative mRNA relative expression levels of FOLR3 by reverse transcription-quantitative PCR. (D) CCK-8 for 0, 24, 48, 72 and 96 h. (E) Colony forming ability evaluated using colony formation assay and (F) quantification (magnification, x4). (G) Cell migratory capacity analyzed using a wound healing assay and (H) quantification (magnification, x20). (I) Invasive potential determined using Transwell invasion assay and (J) quantification (magnification, x10). *P<0.05, **P<0.01, ***P<0.001 and ****P<0.0001. FOLR3, folate receptor γ; CCK-8, Cell Counting Kit-8; NC, negative control.

and mechanisms in thyroid cancer remain to be elucidated in future studies (44-47). Currently, most folate receptor-targeted drugs and diagnostic technologies focus on FOLR1. High expression level of membrane-bound FOLR1 is a recognized predictor of targeted therapy sensitivity, while soluble FOLR3 levels may be associated with treatment resistance (45,48). The

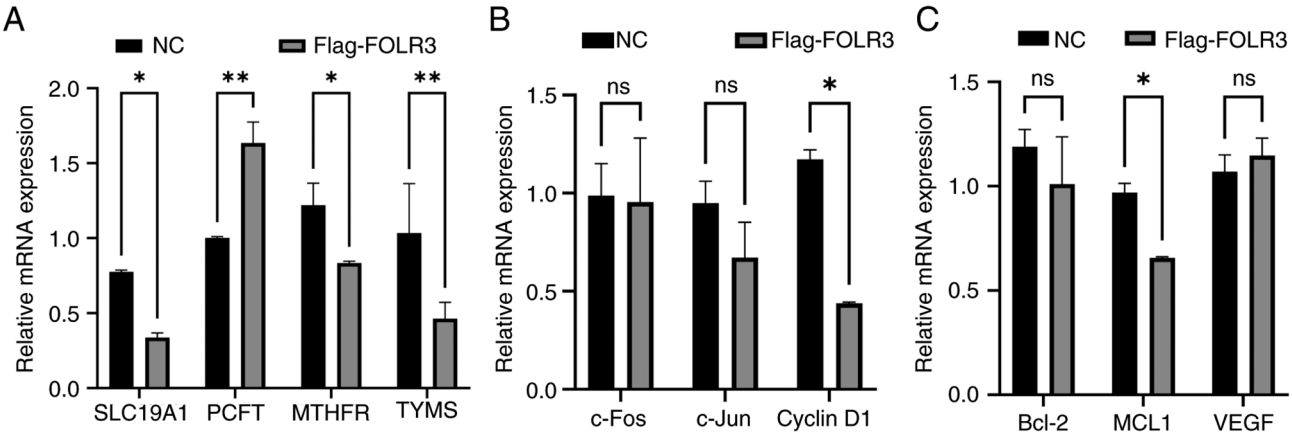

Figure 5. FOLR3 overexpression promotes folate metabolism and activates oncogenic signaling pathways in thyroid cancer cells. (A) mRNA expression levels of folate metabolism-related genes (SLC19A1, PCFT, MTHFR and TYMS) after FOLR3 overexpression. (B) mRNA expression levels of MAPK pathway downstream genes (c-Fos, c-Jun and cyclin D1) after FOLR3 overexpression. (C) mRNA expression levels of STAT3 pathway downstream genes after FOLR3 overexpression. *P<0.05 and **P<0.01. ns, not significant; FOLR3, folate receptor γ; TYMS, thymidylate synthase; MTHFR, methylenetetrahydrofolate reductase; SLC19A1, solute carrier family 19 member 1; PCFT, proton-coupled folate transporter; c-FOS, Fos proto-oncogenes, AP-1 transcription factor subunit; MCL1, myeloid cell leukemia-1; NC, negative control.

present study identified reduced expression levels of FOLR3 in thyroid cancer, which appears to specifically reflect malignant progression. FOLR3 may influence carcinogenesis through the folate metabolism-signaling axis and modulate local folate availability via epigenetic regulation of soluble folate pools. Further research could explore 'metabolic compensation' strategies using FOLR3 for aggressive thyroid cancer with poor prognosis, highlighting its therapeutic potential. Since FOLR3 is secreted into the bloodstream, it may serve as a non-invasive biomarker in liquid biopsies. For instance, hypomethylation of FOLR3 in the blood of patients with lung cancer suggests its utility as an early diagnostic marker (12).

However, whether FOLR3 can be used for thyroid cancer diagnosis via liquid biopsy requires further validation. Theoretically, blood-based FOLR3 levels may be associated with tumor burden, metabolic activity or disease stage. While FOLR3 alone may not be sufficient for diagnosis, its combination with other markers, such as CA-125, human epididymis protein 4 or circulating tumor DNA mutations, could significantly enhance diagnostic accuracy and sensitivity (49-51). Although the present study provided evidence supporting the tumor-suppressive role of FOLR3 in thyroid cancer, several limitations should be acknowledged. The clinical samples, despite having detailed pathological annotations, were obtained from a single center with a limited cohort size (n=293). Validation in a larger, multi-center cohort is warranted to enhance the statistical power and generalizability of the association between FOLR3 expression and clinicopathological characteristics. Furthermore, the lack of *in vivo* validation using animal models, such as xenograft or orthotopic models, restricts the comprehensive confirmation of its tumor-suppressive function within a more complex physiological context. The present study primarily focused on the role of FOLR3 in thyroid cancer itself, while its interactions with the tumor immune microenvironment, stromal components and other folate metabolism-related genes have not been extensively investigated. In the future, FOLR3 may have the potential to serve as a diagnostic biomarker and a novel therapeutic target in thyroid cancer; however, further research is warranted to explore its clinical applicability in both treatment and prognosis assessment.

Acknowledgements

The authors would like to thank Mr Xiaokai Liu (Chi Feng No. 2 Senior High School, Chifeng, China) for their assistance in polishing the English language and grammar of the manuscript.

Funding

The present study was supported by the Chifeng Municipal Natural Science Foundation (grant no. SZR2023063).

Availability of data and materials

The data generated in the present study may be requested from the corresponding author.

Authors' contributions

JC, YL and LT conceptualized the present study; JC, YL and XD devised the methodology. JC and XD; JC, YL and XD validated the data. JC, LH, YL and LT analyzed data. JC, YL and BL performed the experiments. YL and LT prepared the resources. JC, YL and XD curated the data. JC, YL and XD visualized the data. JC, YL and XD prepared the original draft of the manuscript. JC, YL, LH and LT reviewed and edited the manuscript. LT supervised the present study. YL and LT contributed to project administration. All authors read and approved the final manuscript. JC and YL confirm the authenticity of all the raw data.

Ethics approval and consent to participate

The present study was approved by the Scientific Research Ethics Committee of Chifeng City Hospital (approval no.

CK2023037; approval on 20 April 2023; Chifeng, China). The present study is retrospective in nature, and the informed consent requirement was waived by the Ethics Committee.

Patient consent for publication

Not applicable.

Competing interests

The authors declare that they have no competing interests.

Use of artificial intelligence tools

During the preparation of this work, artificial intelligence tools were used to improve the readability and language of the manuscript, and subsequently, the authors revised and edited the content produced by the artificial intelligence tools as necessary, taking full responsibility for the ultimate content of the present manuscript.

References

1. Chen MM, Luu M, Sacks WL, Orloff L, Wallner LP, Clair JM, Pitt SC, Ho AS and Zumsteg ZS: Trends in incidence, metastasis, and mortality from thyroid cancer in the USA from 1975 to 2019: A population-based study of age, period, and cohort effects. Lancet Diabetes Endocrinol 13: 188-195, 2025.
2. Siegel RL, Giaquinto AN and Jemal A: Cancer statistics, 2024. CA Cancer J Clin 74: 12-49, 2024.
3. Boucai L, Zafereo M and Cabanillas ME: Thyroid cancer: A review. JAMA 331: 425-435, 2024.
4. Shen F, Wu M, Ross JF, Miller D and Ratnam M: Folate receptor type gamma is primarily a secretory protein due to lack of an efficient signal for glycosylphosphatidylinositol modification: Protein characterization and cell type specificity. Biochemistry 34: 5660-5665, 1995.
5. Wang HC, Huo YN and Lee WS: Folic acid prevents the progesterone-promoted proliferation and migration in breast cancer cell lines. Eur J Nutr 59: 2333-2344, 2020.
6. Moazzen S, Dolatkhah R, Tabrizi JS, Shaarbafi J, Alizadeh BZ, de Bock GH and Dastgiri S: Folic acid intake and folate status and colorectal cancer risk: A systematic review and meta-analysis. Clin Nutr 37: 1926-1934, 2018.
7. Sadeghi Jam Z, Tafvizi F, Khodarahmi P, Jafari P and Baghbani-Arani F: Cisplatin-loaded UiO-66-NH2 functionalized with folic acid enhances apoptotic activity and antiproliferative effects in MDA-MB-231 breast and A2780 ovarian cancer cells: An in vitro study. Heliyon 11: e42685, 2025.
8. Crider KS, Yang TP, Berry RJ and Bailey LB: Folate and DNA methylation: A review of molecular mechanisms and the evidence for Folate's role. Adv Nutr 3: 21-38, 2012.
9. Petersen LF, Brockton NT, Bakkar A, Liu S, Wen J, Weljie AM and Bismar TA: Elevated physiological levels of folic acid can increase in vitro growth and invasiveness of prostate cancer cells. BJU Int 109: 788-795, 2012.
10. Ullevig SL, Bacich DJ, Gutierrez JM, Balarin A, Lobitz CA, O'Keefe DS and Liss MA: Feasibility of dietary folic acid reduction intervention for men on active surveillance for prostate cancer. Clin Nutr ESPEN 44: 270-275, 2021.
11. Li JT, Yang H, Lei MZ, Zhu WP, Su Y, Li KY, Zhu WY, Wang J, Zhang L, Qu J, *et al*: Dietary folate drives methionine metabolism to promote cancer development by stabilizing MAT IIA. Signal Transduct Target Ther 7: 192, 2022.
12. Qu Y, Zhang X, Qiao R, Di F, Song Y, Wang J, Ji L, Zhang J, Gu W, Fang Y, *et al*: Blood FOLR3 methylation dysregulations and heterogeneity in non-small lung cancer highlight its strong associations with lung squamous carcinoma. Respir Res 25: 59, 2024.
13. Holm J and Hansen SI: Characterization of soluble folate receptors (folate binding proteins) in humans. Biological roles and clinical potentials in infection and malignancy. Biochim Biophys Acta Proteins Proteom 1868: 140466, 2020.
14. Wu MH, Luo JD, Wang WC, Chang TH, Hwang WL, Lee KH, Liu SY, Yang JW, Chiou CT, Chang CH and Chiang WF: Risk analysis of malignant potential of oral verrucous hyperplasia: A follow-up study of 269 patients and copy number variation analysis. Head Neck 40: 1046-1056, 2018.
15. Hansen MF, Greibe E, Skovbjerg S, Rohde S, Kristensen AC, Jensen TR, Stentoft C, Kjær KH, Kronborg CS and Martensen PM: Folic acid mediates activation of the pro-oncogene STAT3 via the Folate Receptor alpha. Cell Signal 27: 1356-1368, 2015.
16. Ma Q, Geng K, Xiao P and Zeng L: Identification and prognostic value exploration of radiotherapy sensitivity-Associated genes in Non-Small-cell lung cancer. Biomed Res Int 2021: 5963868, 2021.
17. Zee RY, Rose L, Chasman DI and Ridker PM: Genetic variation of fifteen folate metabolic pathway associated gene loci and the risk of incident head and neck carcinoma: The Women's Genome Health Study. Clin Chim Acta 418: 33-36, 2013.
18. Liao T, Zeng Y, Xu W, Shi X, Shen C, Du Y, Zhang M, Zhang Y, Li L, Ding P, *et al*: A spatially resolved transcriptome landscape during thyroid cancer progression. Cell Rep Med 6: 102043, 2025.
19. Ritchie ME, Phipson B, Wu D, Ritchie ME, Phipson B and Wu D: Limma powers differential expression analyses for RNA-sequencing and microarray studies. Nucleic Acids Res 43: e47, 2015.
20. Wu T, Hu E, Xu S, Chen M, Guo P, Dai Z, Feng T, Zhou L, Tang W, Zhan L, *et al*: clusterProfiler 4.0: A universal enrichment tool for interpreting omics data. Innovation (Camb) 2: 100141, 2021.
21. Li X, Zhang L, Liu C, He Y, Li X, Xu Y, Gu C, Wang X, Wang S, Zhang J and Liu J: Construction of mitochondrial quality regulation genes-related prognostic model based on bulk-RNA-seq analysis in multiple myeloma. Biofactors 51: e2135, 2025.
22. Huang X, Sun Y, Song J, Huang Y, Shi H, Qian A, Cao Y, Zhou Y and Wang Q: Prognostic value of fatty acid metabolism-related genes in colorectal cancer and their potential implications for immunotherapy. Front Immunol 14: 1301452, 2023.
23. Ning X, Li R, Zhang B, Wang Y, Zhou Z, Ji Z, Lyu X and Chen Z: Immune score indicator for the survival of melanoma patients based on tumor microenvironment. Int J Gen Med 14: 10397-10416, 2021.
24. Zhao AY, Unterman A, Abu Hussein NS, Sharma P, Nikola F, Flint J, Yan X, Adams TS, Justet A, Sumida TS, *et al*: Single-cell analysis reveals novel immune perturbations in fibrotic hypersensitivity pneumonitis. Am J Respir Crit Care Med 210: 1252-1266, 2024.
25. Li Y, Li F, Xu L, Shi X, Xue H, Liu J, Bai S, Wu Y, Yang Z, Xue F, *et al*: Single cell analyses reveal the PD-1 blockade response-related immune features in hepatocellular carcinoma. Theranostics 14: 3526-3547, 2024.
26. Jin S, Guerrero-Juarez CF, Zhang L, Chang I, Ramos R, Kuan CH, Myung P, Plikus MV and Nie Q: Inference and analysis of cell-cell communication using CellChat. Nat Commun 12: 1088, 2021.
27. Huang A, Sun Z, Hong H, Yang Y, Chen J, Gao Z and Gu J: Novel hypoxia- and lactate metabolism-related molecular subtyping and prognostic signature for colorectal cancer. J Transl Med 22: 587, 2024.
28. Marrero JA, Kulik LM, Sirlin CB, Zhu AX, Finn RS, Abecassis MM, Roberts LR and Heimbach JK: Diagnosis, staging, and management of hepatocellular carcinoma: 2018 practice guidance by the American association for the study of liver diseases. Hepatology 68: 723-750, 2018.
29. Humphries MP, Maxwell P and Salto-Tellez M: QuPath: The global impact of an open source digital pathology system. Comput Struct Biotechnol J 19: 852-859, 2021.
30. Wen Z, Luo D, Wang S, Rong R, Evers BM, Jia L, Fang Y, Daoud EV, Yang S, Gu Z, *et al*: Deep Learning-Based H-Score quantification of immunohistochemistry-stained images. Mod Pathol 37: 100398, 2024.
31. Siena S, Raghav K, Masuishi T, Yamaguchi K, Nishina T, Elez E, Rodriguez J, Chau I, Di Bartolomeo M, Kawakami H, *et al:* HER2-related biomarkers predict clinical outcomes with trastuzumab deruxtecan treatment in patients with HER2-expressing metastatic colorectal cancer: Biomarker analyses of DESTINY-CRC01. Nat Commun 15: 10213, 2024.
32. Livak KJ and Schmittgen TD: Analysis of relative gene expression data using real-time quantitative PCR and the 2(-Delta Delta C(T)) method. Methods 25: 402-408, 2001.
33. Li M, Hu M, Jiang L, Pei J and Zhu C: Trends in cancer incidence and potential associated factors in China. JAMA Netw Open 7: e2440381, 2024.

34. Miranda-Filho A, Lortet-Tieulent J, Bray F, Cao B, Franceschi S, Vaccarella S and Dal Maso L: Thyroid cancer incidence trends by histology in 25 countries: A population-based study. Lancet Diabetes Endocrinol 9: 225-234, 2021.
35. Tao Z, Ding Z, Guo B, Fan Y and Deng X: Influence factors and survival outcomes of different invasion sites in locally advanced thyroid cancer and new site-based risk stratification system. Endocrine 88: 501-510, 2025.
36. Yu X, Deng Q, Gao X, He L, Hu D and Yang L: A prognostic nomogram for distant metastasis in thyroid cancer patients without lymph node metastasis. Front Endocrinol (Lausanne) 16: 1523785, 2025.
37. Lv X and Yu X: Signatures and prognostic values of related immune targets in tongue cancer. Front Surg 9: 952389, 2023.
38. Davidson B, Abeler VM, Førsund M, Holth A, Yang Y, Kobayashi Y, Chen L, Kristensen GB, Shih IeM and Wang TL: Gene expression signatures of primary and metastatic uterine leiomyosarcoma. Hum Pathol 45: 691-700, 2014.
39. Bin-Alee F, Arayataweegool A, Buranapraditkun S, Mahattanasakul P, Tangjaturonrasme N, Hirankarn N, Mutirangura A and Kitkumthorn N: Transcriptomic analysis of peripheral blood mononuclear cells in head and neck squamous cell carcinoma patients. Oral Dis 27: 1394-1402, 2021.
40. Qiao R, Di F, Wang J, Wei Y, Xu T, Dai L, Gu W, Han B and Yang R: Identification of FUT7 hypomethylation as the blood biomarker in the prediction of early-stage lung cancer. J Genet Genomics 50: 573-581, 2023.
41. Li L, Wang R, He S, Shen X, Kong F, Li S, Zhao H, Lian M and Fang J: The identification of induction chemo-sensitivity genes of laryngeal squamous cell carcinoma and their clinical utilization. Eur Arch Otorhinolaryngol 275: 2773-2781, 2018.
42. O'Byrne MR, Au KS, Morrison AC, Lin JI, Fletcher JM, Ostermaier KK, Tyerman GH, Doebel S and Northrup H: Association of folate receptor (FOLR1, FOLR2, FOLR3) and reduced folate carrier (SLC19A1) genes with meningomyelocele. Birth Defects Res A Clin Mol Teratol 88: 689-694, 2010.
43. Grarup N, Sulem P, Sandholt CH, Thorleifsson G, Ahluwalia TS, Steinthorsdottir V, Bjarnason H, Gudbjartsson DF, Magnusson OT, Sparsø T, *et al*: Genetic architecture of vitamin B12 and folate levels uncovered applying deeply sequenced large datasets. PLoS Genet 9: e1003530, 2013.
44. Nawaz FZ and Kipreos ET: Emerging roles for folate receptor FOLR1 in signaling and cancer. Trends Endocrinol Metab 33: 159-174, 2022.
45. Mai J, Wu L, Yang L, Sun T, Liu X, Yin R, Jiang Y, Li J and Li Q: Therapeutic strategies targeting folate receptor α for ovarian cancer. Front Immunol 14: 1254532, 2023.
46. Matsunaga Y, Yamaoka T, Ohba M, Miura S, Masuda H, Sangai T, Takimoto M, Nakamura S and Tsurutani J: Novel Anti-FOLR1 Antibody-drug conjugate MORAb-202 in breast cancer and non-Small cell lung cancer cells. Antibodies (Basel) 10: 6, 2021.
47. Chen CI, Li WS, Chen HP, Liu KW, Tsai CJ, Hung WJ and Yang CC: High expression of folate receptor alpha (FOLR1) is associated with aggressive tumor behavior, poor response to chemoradiotherapy, and worse survival in rectal cancer. Technol Cancer Res Treat 21: 15330338221141795, 2022.
48. Varaganti P, Buddolla V, Lakshmi BA and Kim YJ: Recent advances in using folate receptor 1 (FOLR1) for cancer diagnosis and treatment, with an emphasis on cancers that affect women. Life Sci 326: 121802M, 2023.
49. Medina JE, Annapragada AV, Lof P, Short S, Bartolomucci AL, Mathios D, Koul S, Niknafs N, Noë M, Foda ZH, *et al*: Early detection of ovarian cancer Using Cell-Free DNA fragmentomes and protein biomarkers. Cancer Discov 15: 105-118, 2025.
50. Muinao T, Deka Boruah HP and Pal M: Multi-biomarker panel signature as the key to diagnosis of ovarian cancer. Heliyon 5: e02826, 2019.
51. Heitz F, Lakis S, Harter P, Heikaus S, Sehouli J, Talwar J, Menon R, Ataseven B, Bertrand M, Schneider S, *et al*: Cell-free tumor DNA, CA125 and HE4 for the objective assessment of tumor burden in patients with advanced high-grade serous ovarian cancer. PLoS One 17: e0262770, 2022.